 doi:10.20944/preprints201802.0014.v1

Article

Photovoltaic Cell and Module I-V Characteristic Approximation Using Bézier Curves

Roland Szabo [1] and Aurel Gontean *

[1] Applied Electronics Department, Politehnica University Timisoara, Timisoara 300006, Romania; roland.szabo@upt.ro (R.S.); aurel.gontean@upt.ro (A.G.)
* Correspondence: aurel.gontean@upt.ro; Tel.: +40-745-121-383

Abstract: The aim of this work is to introduce new ways to model the I-V characteristic of a PV cell or PV module using straight lines and Bézier curves. This is a complete novel approach, Bézier curves being previously used mainly for computer graphics. The I-V characteristic is divided in three sections, modeled with lines and a quadratic Bézier curve in the first case and with three cubic Bézier curves in the second case. The result proves to be accurate and relies on the fundamental points usually present in the PV cell datasheets: V_{oc} (the open circuit voltage), I_{sc} (the short circuit current), V_{mp} (the maximum power corresponding voltage) and I_{mp} (the maximum power corresponding current) and the parasitic resistances R_{sh0} (shunt resistance at I_{sc}) and R_{s0} (series resistance at V_{oc}). The proposed algorithm completely defines all the implied control points and the error is analyzed. The proposed method is validated for different temperatures and irradiances. The model is finally compared and validated using the least squares fitting method.

Keywords: PV cell; I-V characteristic; model; simulation; interpolation; Bézier curve; control points; least squares fitting method

1. Introduction

The forecast of the total PV installs, offered by Bloomberg New Energy Finance (BNEF) predicts an optimistic growth at 111 GW in 2018, rising to 121 GW in 2019, along with a polysilicon factory grow boom and module prices drop to US$0.30/W [1], [2]. This robust growth explains the high interest in PV research, modeling and simulation – along with design and development of PV equipment.

The electrical characteristics of the PV cell and PV modules have been of interest for several decades, and different models have been proposed. Phang and Chan [3] were among the first to propose a solution for PV cell parameter extraction. Villalva et al. [4] developed an algorithm to find the parameters defining the I-V characteristic for the single diode model of a PV cell, using the Newton-Raphson method and imposing a minimum error threshold for the maximum power point. Cubas et al. [5] used the Lambert W-Function for finding the solar panel equivalent circuit parameters and they also proposed an LTSpice model according to their findings. Temperature influence is studied by Chander et al. [6].

In a recent work, Cuce et al. [7] claim a good accuracy for their electrical model for a PV module and they also discuss energy and exergy efficiency as a reliable substitute for the fill factor. In our previous work [8], we proposed a complete SPICE model including all the parameters variation and selfheating. All the aforementioned works use an electrical model to describe the behavior of the circuit and rely on a specific circuit to generate the I-V characteristic of the PV cell or module.

This paper introduces a new approach. This time, the cell or module are not involved at the electrical level, being defined by just the specific points P_{sc}, P_{mp}, P_{oc} and by the parallel and series resistances R_{sh0} and R_{s0}, specified at I_{sc} and V_{oc}, respectively. Carefully inspection of the typical I-V characteristic of the PV module or PV cell (Figure 1a and 1b) shows a similar pattern in all curves. Our aim was to find a way to model it using smooth curves and datasheet information currently available.

Preprints (www.preprints.org) | NOT PEER-REVIEWED | Posted: 2 February 2018 doi:10.20944/preprints201802.0014.v1

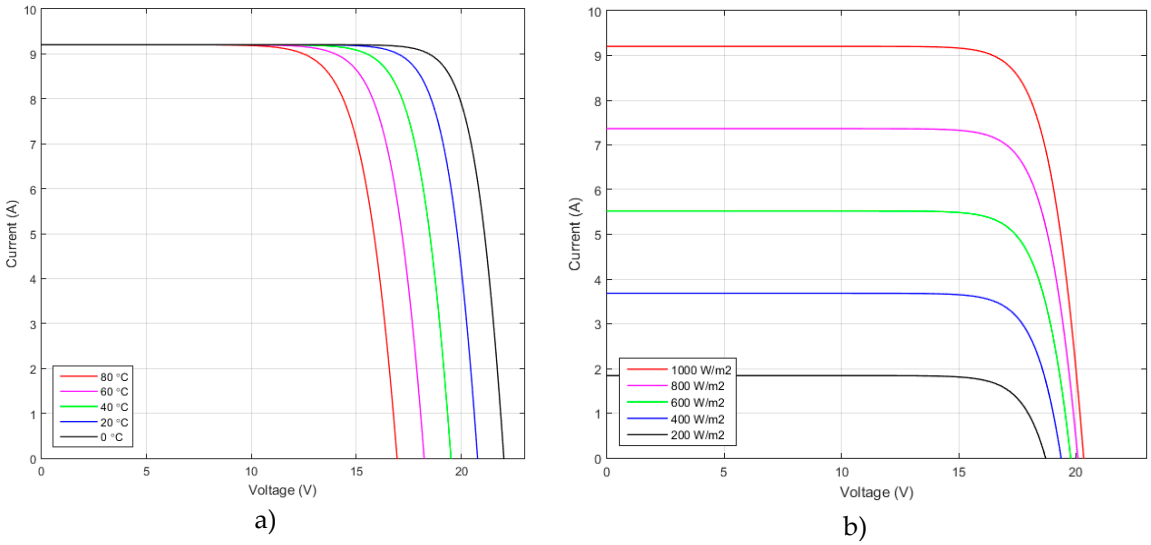

Figure 1. Typical PV module I-V characteristics, with 30 cells connected in series. a) at different temperatures (0 - 80 °C). b) At different irradiances (200 – 1000 W/m^2).

Bernstein polynomials have been studied since the beginning of the 20th century and they form the foundation for Bézier curves [9]. The core applications for graphics came first in 1959 when the French mathematician Paul de Casteljau developed an algorithm able to evaluate a family of specific curves at Citroën. In 1962 the French engineer Pierre Bézier also used them to design automobile bodies at Renault and afterwards they got wide acceptance [10].

Bézier curves are largely used in computer graphics [11, 12] and also in time domain for smoothing the trajectory of the robotic arms, for an accurate gluing or welding path or for trajectory generation [13]. Further development for shape representation is proposed by Jalba et al. [14].

The current proposal analyses the use of Bézier curves [15] in order to accurately represent the I-V characteristic of a PV cell or module. A complete mathematical solution is provided, separately validated for a PV cell and a PV module and the error is analyzed. The results are also studied for different temperature and irradiances and finally compared with the ones offered by the least squares fitting method.

The remainder of this paper is organized as follows: Section 2 briefly analyzes the definition of the quadratic and cubic Bézier curves and their equations, focusing on the basic knowledge needed in the subsequent paragraphs. Section 3 deals with the information usually provided by the PV cell or module manufacturers in their datasheets. The proposed models are covered in Section 4, with Section 4.1 introducing the approximation with two segments and one quadratic Bézier curve, while Section 4.2 deals with the better approximation based on three Bézier cubic curves. The models are rated at the reference temperature, 25°C. The results are also compared with the least squares fitting method in Section 4.3. In Section 4.4 the influence of the external parameters is analyzed. Discussion and conclusions are provided in the next Sections.

2. Definition of the Bézier Curves

A quadratic Bézier curve (Figure 2) can be specified by three control points [10]: the curve goes through the ends P_0 and P_2 and approximates P_1.

Preprints (www.preprints.org) | NOT PEER-REVIEWED | Posted: 2 February 2018 doi:10.20944/preprints201802.0014.v1

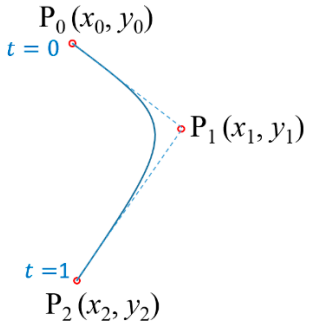

Figure 2. A quadratic Bézier curve representation. P_0 and P_2 are the end points, the control point P_1 is approximated and the curve is tangent to $\overline{P_0P_1}$ and $\overline{P_2P_1}$ segments at P_0 and P_2 respectively.

The curve equation is as follows [15]:

$$B_2(t) = (1-t)^2P_0 + 2t(1-t)P_1 + t^2P_2 \quad (1)$$

where t varies between 0 and 1. Equation (1) can be expressed for the x and y coordinates:

$$\begin{cases} x(t) = (1-t)^2x_0 + 2t(1-t)x_1 + t^2x_2 \\ y(t) = (1-t)^2y_0 + 2t(1-t)y_1 + t^2y_2 \end{cases} \quad (2)$$

The derivative of (1) is:

$$B_2'(t) = 2(1-t)(P_1 - P_0) + 2t(P_2 - P_1) \quad (3)$$

At the end points, (3) becomes (4):

$$\begin{cases} B_2'(t)|_{t=0} = 2P_1 - 2P_0 \\ B_2'(t)|_{t=1} = 2P_2 - 2P_1 \end{cases} \quad (4)$$

A cubic Bézier curve (Figure 3) can be specified by four control points [10]: the curve goes through the ends P_0 and P_3 and approximates P_1 and P_2. The analytical expression of the curve is a cubic polynomial. The curve is tangent at P_0 to $\overline{P_0P_1}$ and at P_3 to $\overline{P_3P_2}$.

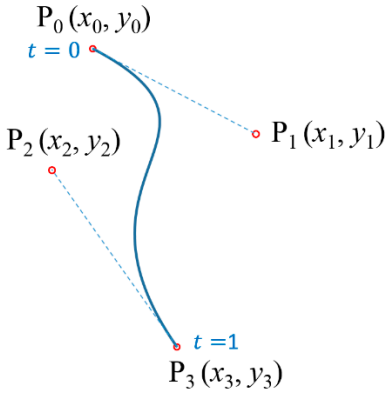

Figure 3. A cubic Bézier curve representation. P_0 and P_3 are the end points, the control points P_1 and P_2 are approximated and the curve is tangent to $\overline{P_0P_1}$ and $\overline{P_2P_1}$ segments at P_0 and P_3 respectively.

The equation for the Bézier cubic curve is [15]:

$$B_3(t) = (1-t)^3P_0 + 3t(1-t)^2P_1 + 3t^2(1-t)P_2 + t^3P_3 \quad (5)$$

The previous equation can be expressed for the x and y coordinates:

Preprints (www.preprints.org) | NOT PEER-REVIEWED | Posted: 2 February 2018 doi:10.20944/preprints201802.0014.v1

$$\begin{cases} x(t) = (1-t)^3 x_0 + 3t(1-t)^2 x_1 + 3t^2(1-t)x_2 + t^3 x_3 \\ y(t) = (1-t)^3 y_0 + 3t(1-t)^2 y_1 + 3t^2(1-t)y_2 + t^3 y_3 \end{cases} \quad (6)$$

The derivative of (5) is:

$$B_3'(t) = 3(1-t)^2(P_1 - P_0) + 6t(1-t)(P_2 - P_1) + 3t^2(P_3 - P_2) \quad (7)$$

At the end points, (7) becomes (8):

$$\begin{cases} B_3'(t)|_{t=0} = 3P_1 - 3P_0 \\ B_3'(t)|_{t=1} = 3P_3 - 3P_2 \end{cases} \quad (8)$$

3. Materials and Methods

The PV cell used in our work is a high efficiency, silicon monocrystalline 156 x 156 mm² cell [16] and has the main characteristics summarized in Table 1.

Table 1. PV Cell main specifications on STC (1000W/m², AM 1.5, 25°C)

Symbol	Description	Value
$V_{oc,cell,ref}$	Cell open circuit voltage	0.699 V
$I_{sc,ref}$	Short circuit current	9.207 A
V_{mp}	Maximum power voltage	0.572 V
I_{mp}	Maximum power current	8.756 A
R_{sh0}	Shunt resistance at I_{sc}	73.19 Ω
R_{s0}	Series resistance at V_{oc}	3.8 mΩ

The MSMD290AS-36_EU Monocrystalline PV module [17] is well documented and studied by Cubas et al. [5]. Its main electrical data is listed in Table 2 and this information will be used in Section 4.4 to evaluate the influence of the temperature and irradiance to our Bézier curves based model.

Table 2. MSMD290AS-36_EU Module main specifications on STC (1000W/m², AM 1.5, 25°C)

Symbol	Description	Value
$V_{oc,module,ref}$	Cell open circuit voltage	44.68 V
$I_{sc,ref}$	Short circuit current	8.24 A
V_{mp}	Maximum power voltage	37.66 V
I_{mp}	Maximum power current	7.70 A
R_{sh0}	Shunt resistance at I_{sc}	316 Ω
R_{s0}	Series resistance at V_{oc}	130 mΩ
k_I	Current temperature coefficient	3.296 mA/K
k_V	Voltage temperature coefficient	-146.256 mV/K
n_s	Number of series cell	72

For studying and representing Bézier curves, an interesting application which allows draggable control points was developed by Mugnaini [18]. For computing the coordinates on the curves we used the Kronecker tensor product found as in [19]. An example for Bézier least square fitting method is given in [20].

4. Results

It must be stressed out that all the physical actual values involved in sections 4.1, 4.2 and 4.3 are specified at 25°C, being reference values. The irradiance is also standard (1000 $^{W}/_{m^2}$). As it will be demonstrated in section 4.4., the same method is suitable for different temperatures and irradiances.

Preprints (www.preprints.org) | NOT PEER-REVIEWED | Posted: 2 February 2018 doi:10.20944/preprints201802.0014.v1

4.1. I-V Characteristic approximation with two segments and a quadratic Bézier Curve

The first approximation implies five control points: $P_{sc}(0, I_{sc}), P_a(x_a, y_a), P_b(x_b, y_b), P_c(x_c, y_c)$ and $P_{oc}(V_{oc}, 0)$ and is made of two segment lines $\overline{I_{sc}P_a}$ and $\overline{P_bV_{oc}}$ and one quadratic Bézier curve defined by the endpoints P_a and P_b and the control point P_c (figure 4).

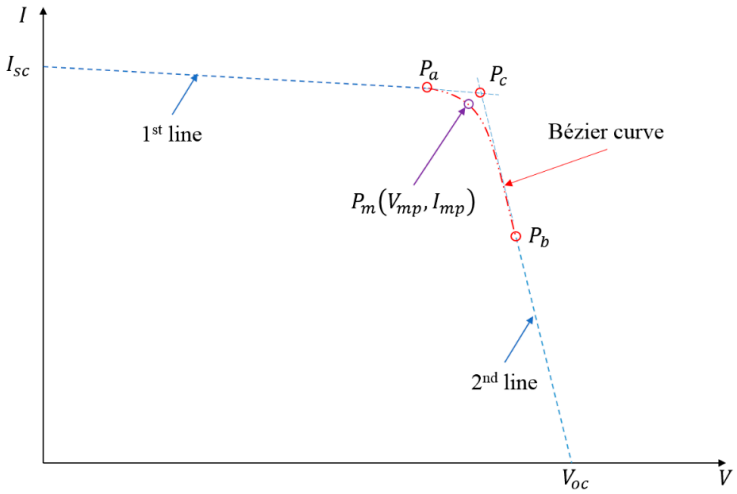

Figure 4. Projected PV cell I-V characteristic approximation with two straight line segments and one quadratic Bézier curve.

It has already been proven [3] that the slopes of the lines can be written as (9) and (10):

$$\left.\frac{dI}{dV}\right|_{V=0} = -\frac{1}{R_{sh0}} \tag{9}$$

$$\left.\frac{dI}{dV}\right|_{V=V_{oc}} = -\frac{1}{R_{s0}} \tag{10}$$

Thus, the equation for first line is (11):

$$I = I_{sc} - \frac{V}{R_{sh0}} \tag{11}$$

By choosing x_a in the linear region (eg $0.6V_{oc}$), one can find y_a from the above equation, so P_a is completely defined.

For the second line, the next equation is valid (12):

$$I = \frac{V_{oc} - V}{R_{s0}} \tag{12}$$

The $P_c(V_c, I_c)$ control point has therefore the coordinates defined by (13):

$$\left(x_c = V_c = \frac{V_{oc}R_{sh0} - I_{sc}R_{sh0}R_{s0}}{R_{sh0} - R_{s0}}, y_c = I_c = \frac{I_{sc}R_{sh0} - V_{oc}}{R_{sh0} - R_{s0}}\right) \tag{13}$$

For x_b, it must be emphasized that its position is on the end of the curve, a realistic value being $0.9V_{oc}$. The maximum power point is positioned on the second curve, so solving (14) gives t_{mp}:

$$t_{mp}^2(x_a + x_b - 2x_c) + 2t_{mp}(x_c - x_a) + x_a - V_{mp} = 0 \tag{14}$$

Replacing the positive solution for t_{mp} in (2) yields y_b as in (15):

Preprints (www.preprints.org) | NOT PEER-REVIEWED | Posted: 2 February 2018 doi:10.20944/preprints201802.0014.v1

$$y_b = \frac{(2t_{mp} - t_{mp}^2 - 1)y_a + 2t_{mp}(t_{mp} - 1)y_c + I_{mp}}{t_{mp}^2} \quad (15)$$

Now all the control points of the plot are completely defined. The results are summarized in Table 3. The application code written for the coordinate finding can be found here: http://tess.upt.ro.

Table 3. The control point coordinates when using two lines and one quadratic Bézier curve

Point	x coordinate (V)	y coordinate (A)
First line segment		
P_{sc}	0	9.207
P_a	0.4893	9.2003
Quadratic Bézier Curve		
P_a	0.4893	9.2003
P_c	0.6070	9.1987
P_b	0.6291	7.0181
Second line segment		
P_b	0.6291	7.0181
P_{oc}	0.699	0

The final plot is represented in Figure 5, where one can observe an excellent correspondence between the actual PV cell I-V characteristic, represented with black dots and the $\overline{P_{sc}P_a}$ segment (blue line), a fair correlation for the second range, approximated by the Bézier quadratic curve (red line) and some modest results in the third region (magenta line).

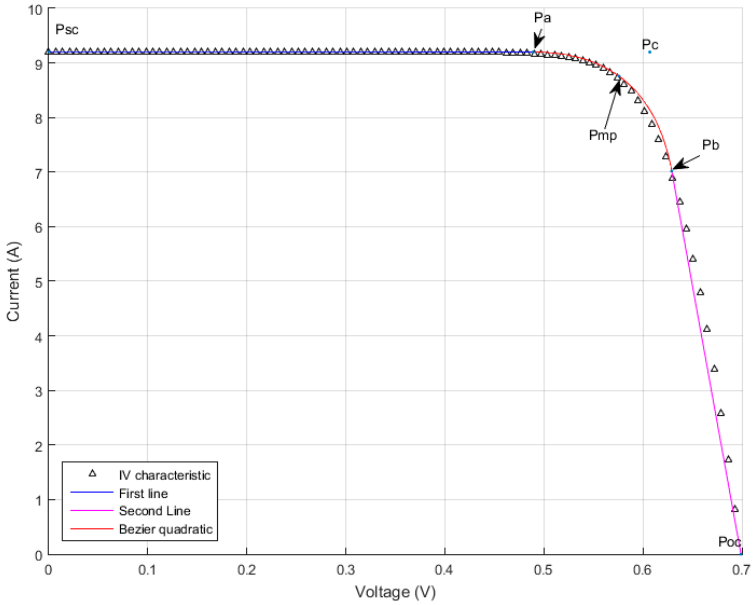

Figure 5. PV cell I-V characteristic approximation with two straight lines and one quadratic Bézier curve – results.

The same conclusion arises from Figure 6, where the relative error has been plotted. It is worth mentioning that although the relative error is quite high above 0.64 V ($0.92V_{oc}$), the absolute error is in fact less than 0.7 A in a region where the cell normally should not operate.

Preprints (www.preprints.org) | NOT PEER-REVIEWED | Posted: 2 February 2018 doi:10.20944/preprints201802.0014.v1

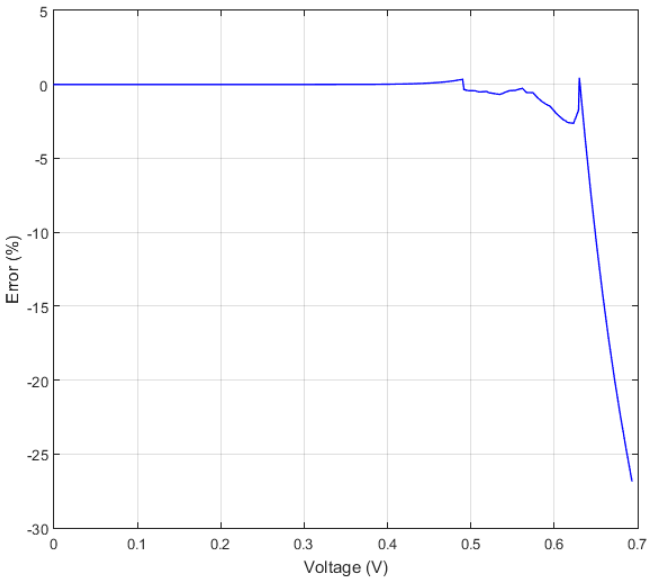

Figure 6. Approximation errors are high over 0.64 V.

Looking for a more accurate model is the reason we came up with the second scenario, where the I-V characteristic is entirely modeled with cubic Bézier curves.

4.2. I-V Characteristic approximation with three cubic Bézier curves

In order to have a general solution, we analyzed the case where all three regions are covered with cubic Bézier curves. This implies 12 control points (Figure 7), i.e. 24 coordinates to be found.

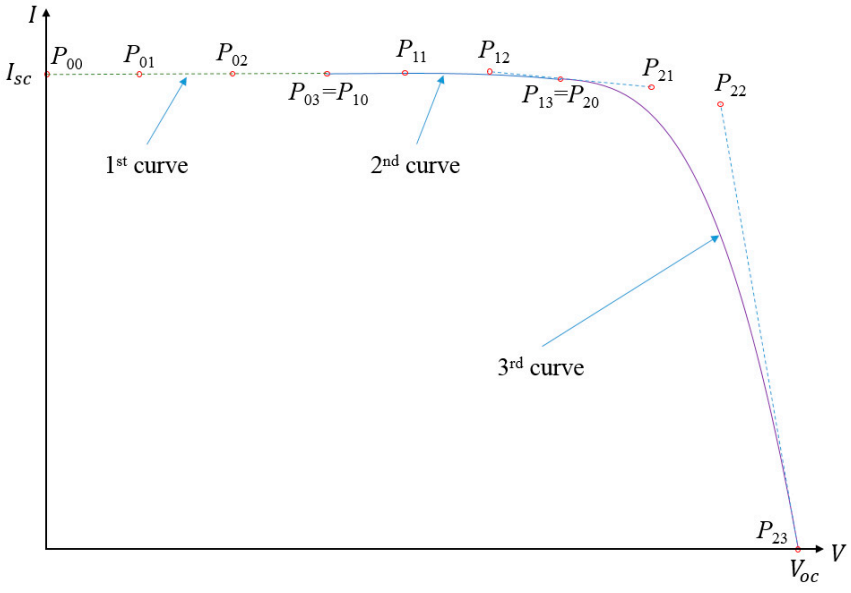

Figure 7. Projected PV cell I-V characteristic approximation with three cubic Bézier curves.

The first curve, represented in Figure 8, is described by the control points $P_{00}(0, I_{sc}), P_{01}, P_{02}$ and P_{03}. It turns out that the linear approximation of the first region of the I-V curve has an error below 0.5% if $P_{03x} = {V_{oc}}/{2}$. During various simulations we have also discovered that all $P_{j,k}$ points can be evenly arranged, with $j = \{1,2\}$; $k = \{1,2,3\}$. This leads to $P_{01x} = {P_{03x}}/{3}$ and $P_{02x} = {2P_{03x}}/{3}$. For the y coordinates, $P_{0ky} = I_{sc} - {P_{0kx}}/{R_{sh0}}$, with $k = \{1,2,3\}$. Now the first curve is completely defined.

Preprints (www.preprints.org) | NOT PEER-REVIEWED | Posted: 2 February 2018 doi:10.20944/preprints201802.0014.v1

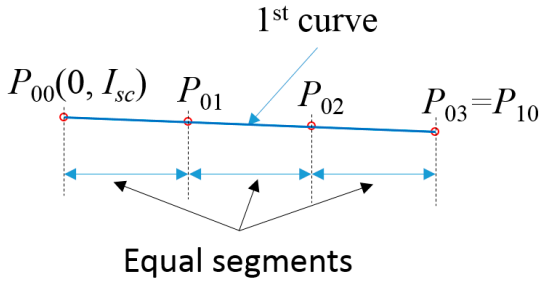

Figure 8. First Bézier curve with the associated control points. The slope is exaggerated for a better understanding.

The second curve (Figure 7) is described by the control points $P_{10} = P_{03}, P_{11}, P_{12}$ and P_{13}. We observed that $P_{13x} = 0.75V_{oc}$ offers a very good fit of the curve for this type of PV cell. With the same evenly arrangement for the x coordinates, $P_{1kx} = P_{10x} + {k(P_{13x} - P_{10x})}/{3}$, with $k = \{1,2\}$. $P_{11}$is also located in the linear region of the I-V curve, so $P_{11y} = P_{03y} - {P_{11x}}/{R_{sh0}}$. This leaves P_{12y} and P_{13y} as unknowns at this stage.

The third curve (Figure 7) is described by the control points $P_{20} = P_{13}, P_{21}, P_{22}$ and $P_{23}(V_{oc}, 0)$. Using the same assumptions as for the second curve, $P_{2kx} = P_{20x} + {k(P_{23x} - P_{20x})}/{3}$, with $k = \{1,2\}$. It is obvious that $P_{20x} = P_{13x}$ and $P_{23x} = V_{oc}$. The segment $\overline{P_{22}P_{23}}$ is tangent to the curve at the point P_{23}, so $P_{22y} = {(V_{oc} - P_{22x})}/{R_{s0}}$. This leaves P_{21y} as an additional unknown at this step.

For continuity reasons, $\overline{P_{12}P_{13}}$ and $\overline{P_{20}P_{21}}$ segments belong to the same line. This implies that the derivatives of the second curve at P_{13} and of the third curve at P_{20} are equal (16):

$$3P_{13y} - 3P_{12y} = 3P_{21y} - 3P_{20y} \tag{16}$$

Which means that:

$$P_{21y} = 2P_{13y} - P_{12y} \tag{17}$$

The control point P_{11} is placed on the second curve, so (18) can be written:

$$V_{11} = P_{11x} = (1 - t_{11})^3 P_{10x} + 3t_{11}(1 - t_{11})^2 P_{11x} + 3t_{11}^2(1 - t_{11})P_{12x} + t_{11}^3 P_{13x} \tag{18}$$

Solving the previous equation and keeping only the real solution for t_{11}, (19) is also valid:

$$I_{11} = P_{11y} = (1 - t_{11})^3 P_{10y} + 3t_{11}(1 - t_{11})^2 P_{11y} + 3t_{11}^2(1 - t_{11})P_{12y} + t_{11}^3 P_{13y} \tag{19}$$

Finally, the graph also goes through the MPP point $P_{mp}(V_{mp}, I_{mp})$, yielding equation (20):

$$V_{mp} = (1 - t_{mp})^3 P_{20x} + 3t_{mp}(1 - t_{mp})^2 P_{21x} + 3t_{mp}^2(1 - t_{mp})P_{22x} + t_{mp}^3 P_{23x} \tag{20}$$

Keeping only the real solution for t_{mp}, (21) is also valid:

$$I_{mp} = (1 - t_{mp})^3 P_{20y} + 3t_{mp}(1 - t_{mp})^2 P_{21y} + 3t_{mp}^2(1 - t_{mp})P_{22y} \tag{21}$$

The linear system made of equations (17), (19) and (21) give the last three unknown coordinates P_{12y}, P_{13y} and P_{21y}. The results are summarized in Table 4. The application code written for coordinate finding can be found here: http://tess.upt.ro.

Preprints (www.preprints.org) | NOT PEER-REVIEWED | Posted: 2 February 2018 doi:10.20944/preprints201802.0014.v1

Table 4. The control point coordinates when using three cubic Bézier curves.

Point	x coordinate (V)	y coordinate (A)
First Bézier cubic curve		
P_{00}	0	9.207
P_{01}	0.1165	9.206
P_{02}	0.2330	9.204
P_{03}	0.3495	9.202
Second Bézier cubic curve		
P_{10}	0.3495	9.202
P_{11}	0.4078	9.197
P_{12}	0.4660	9.210
P_{13}	0.5243	9.074
Third Bézier cubic curve		
P_{20}	0.5243	9.074
P_{21}	0.5825	8.939
P_{22}	0.6408	8.616
P_{23}	0.6990	0

Figure 9 shows the location of the control points with respect to the I-V characteristic of the PV cell. The control points $P_{00}, P_{01}, P_{02}, P_{03} = P_{10}$ and P_{11} are collinear and with P_{mp}, are all being placed on the I-V characteristic.

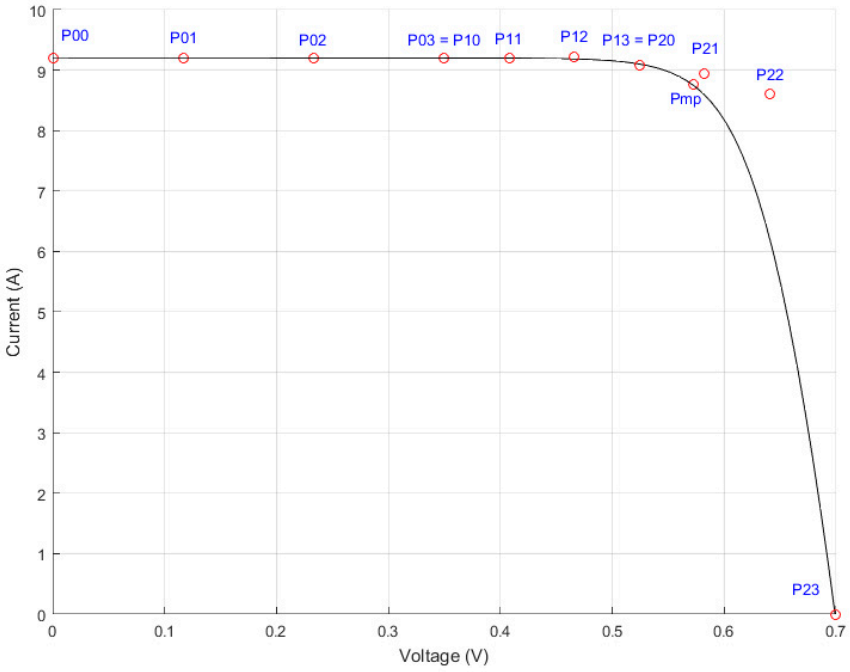

Figure 9. PV cell I-V characteristic (black line, continuous) and the position of the 12 computed control points (red markers).

Figure 10 shows the modeled characteristic (red, green and blue lines) overlapping in most areas with the practical I-V characteristic (black markers). The application code can also be found here: http://tess.upt.ro.

Preprints (www.preprints.org) | NOT PEER-REVIEWED | Posted: 2 February 2018 doi:10.20944/preprints201802.0014.v1

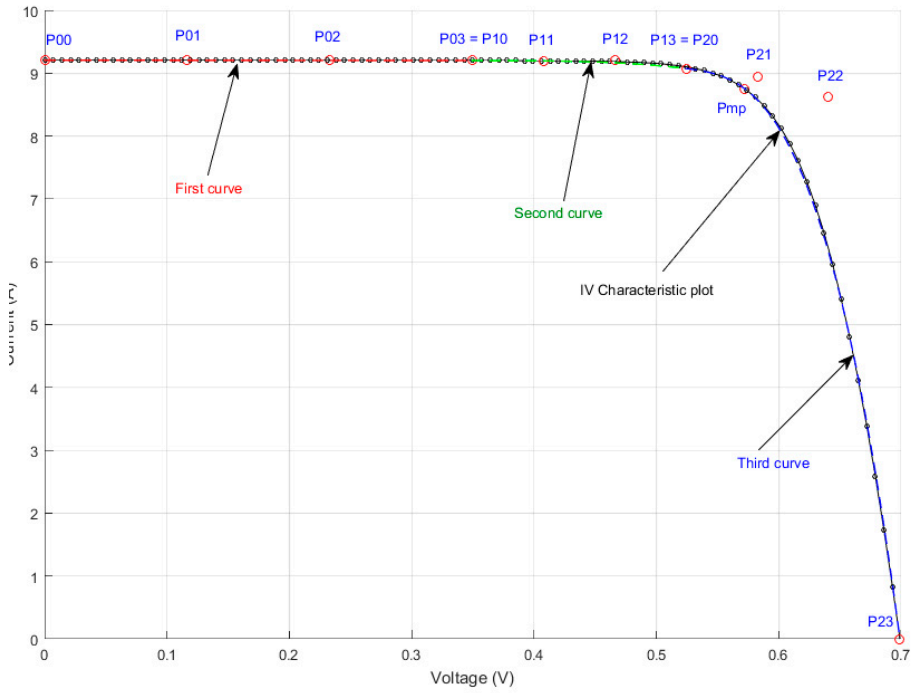

Figure 10. I-V characteristic of a PV cell modeled with three cubic Bézier curves, defined by 12 control points.

The relative error of the Bézier modeled I-V characteristic against the actual data taken from [8] is shown in Figure 11. It must be emphasized that in the 0 … 0.94 V_{oc} range, the relative error is below 1%. Above 0.94 V_{oc} the absolute error is less than 72mA, while the reference $I_{sc} = 9.207$A.

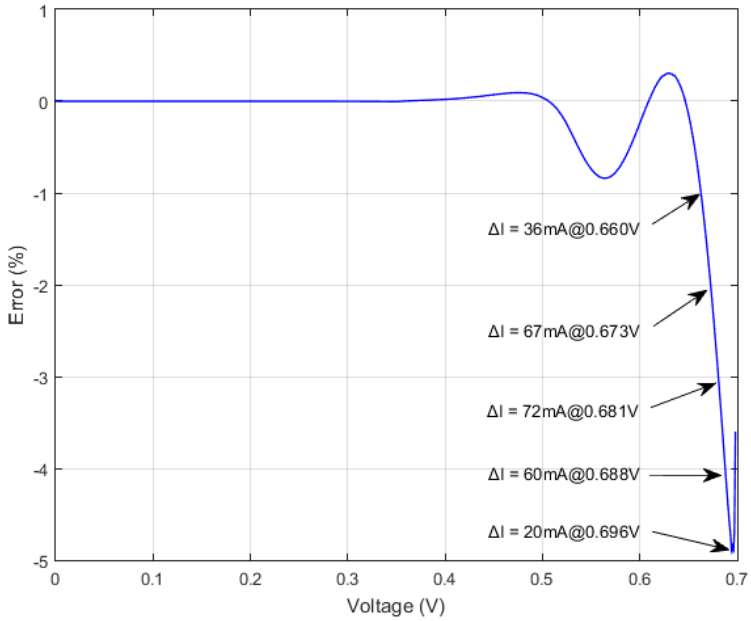

Figure 11. The relative error of our model compared with the actual data. Good performance can be observed in the 0…0.5 V interval and near V_{mp}. Higher errors occur near V_{oc} for low output currents.

4.3. Data fitting using the least squares method

Data fitting using the least squares method is a standard approach in data analysis [21, 22]. A good overview of curve fitting using Bézier cubic curves in image processing is given by Shao et al. in [23], while Zhao et al. [24] extend this method using a genetic algorithm for parameter optimization for Bézier curve fitting. In Section 4.2 we have shown that for the studied PV cell, the best results arise when the x coordinates of the middle end points are set at $0.5V_{oc}$ and $0.75V_{oc}$ respectively. A

Preprints (www.preprints.org) | NOT PEER-REVIEWED | Posted: 2 February 2018 doi:10.20944/preprints201802.0014.v1

similar conclusion arises if the least squares method is used for the same cell modeling. Running the least squares method for the MSMD290AS-36_EU Monocrystalline PV module proved that the minimum error occurs when the control points are set at $0.5V_{oc}$ and $0.8V_{oc}$ respectively. Table 5 summarizes the data fitting results for the same PV cell used in sections 4.1 and 4.2, where the results from the two approaches are very close. The graphical representation of the date fitting is given in Figure 12, where just the endpoints are represented.

Table 5. Control point coordinates comparison. On the left, the least squares method is used for computation, on the right the same values as in Table 4 are listed.

	Least Squares Method		**Proposed Method**	
Point	x coordinate (V)	y coordinate (A)	x coordinate (V)	y coordinate (A)
		First Bézier cubic curve		
P_{00}	0	9.207	0	9.207
P_{01}	0.1165	9.206	0.1165	9.206
P_{02}	0.2330	9.204	0.2330	9.204
P_{03}	0.3495	9.202	0.3495	9.202
		Second Bézier cubic curve		
P_{10}	0.3495	9.202	0.3495	9.202
P_{11}	0.4076	9.183	0.4078	9.197
P_{12}	0.4658	9.245	0.4660	9.210
P_{13}	0.5239	9.103	0.5243	9.074
		Third Bézier cubic curve		
P_{20}	0.5239	9.103	0.5243	9.074
P_{21}	0.5823	8.9646	0.5825	8.939
P_{22}	0.6406	8.6723	0.6408	8.616
P_{23}	0.6990	0.003	0.6990	0

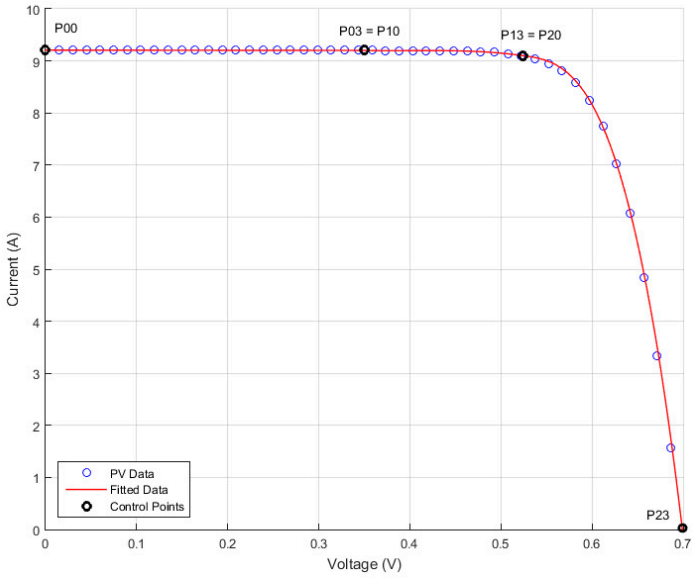

Figure 12. Bézier approximation using the least squares method.

Figure 13 depicts the relative error of the modeled I-V characteristic compared with the actual data taken from our previous work [8]. In the $0 \ldots 0.96V_{oc}$ range, the relative error is below 2%. Furthermore, above $0.96V_{oc}$, the absolute error is less than 66 mA, while the reference short circuit current is 9.207A.

Preprints (www.preprints.org) | NOT PEER-REVIEWED | Posted: 2 February 2018 doi:10.20944/preprints201802.0014.v1

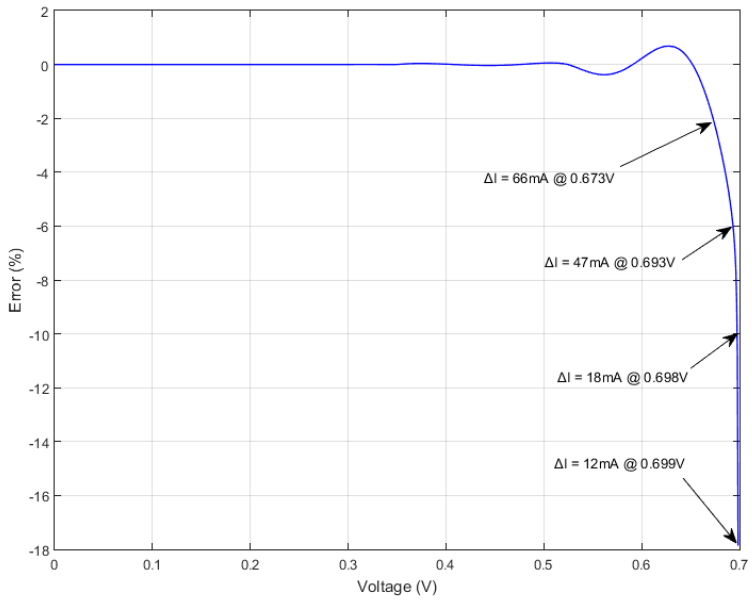

Figure 13. The relative error of the least squares method Bézier based approximation compared with the actual data. The absolute error $\Delta I = I_{Bezier} - I$ is also indicated.

4.4. Parameters variation

In order to finally validate the proposed method, in this section we analyze the temperature and irradiance influence for the MSMD290AS-36_EU Monocrystalline PV module. An extensive study of the parameters influence over the PV cell can be found in [8]. It is important to notice that the Bézier approximation is not related to any of these parameters, just to the specified points P_{sc}, P_{mp}, P_{oc} and the parasitic resistances R_{sh0} and R_{s0} as already stated. The challenge becomes in this case the finding of the new position for the control points and the new values for the parasitic resistances.

Villalva et al. [4] accurately describe the short circuit current variation as in (22):

$$I_{sc} = \left(\frac{R_{sh} + R_s}{R_{sh}} I_{sc,ref} + k_I \Delta T\right) \frac{G}{G_{ref}} \approx \left(I_{sc,ref} + k_I \Delta T\right) \frac{G}{G_{ref}} \tag{22}$$

Ishaque and Salam [7] propose for the $V_{oc,cell}$ the following variation (23):

$$V_{oc,cell} = V_{0c,cell,ref} + a \frac{kT}{q} ln \frac{G}{G_{ref}} + k_v \Delta T \tag{23}$$

Equation (23) proved to be too conservative in this case, as larger $V_{oc,cell}$ variations were observed. A better approximation is the empirical law (24):

$$V_{oc} = 29.579 + 2.1934 \ln G \tag{24}$$

A possible way for defining R_{sh} behavior is suggested in [8], as in (25) with k_{Rsh} estimated as 8 for the best fit.

$$R_{sh} = R_{sh,ref} \left(\frac{T_{ref}}{T}\right)^{k_{Rsh}} \tag{25}$$

For R_s, a linear variation law (26) is given in [8] with $\alpha_{Rs} = -0.01\text{K}^{-1}$, again for the best fit:

$$R_s = R_{s,ref}\left[1 + \alpha_{Rs}\left(T - T_{ref}\right)\right] \tag{26}$$

Preprints (www.preprints.org) | NOT PEER-REVIEWED | Posted: 2 February 2018 doi:10.20944/preprints201802.0014.v1

Figure 14 shows the irradiance influence for the I-V module characteristic, where the approximated data using our proposed method is plotted with solid lines and the experimental data is represented with markers. I_{sc}, V_{oc}, R_{sh} and R_s were computed using (22), (24), (25) and (26) respectively.

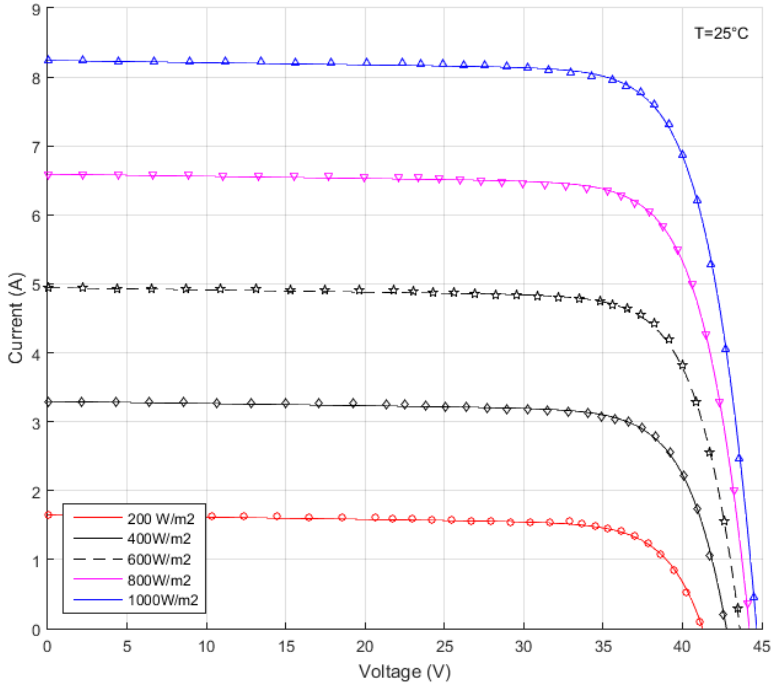

Figure 14. Bézier approximation of the I-V irradiance dependent characteristics for the MSMD290AS-36_EU monocrystalline PV module. The lines represent the computed curves, whereas the markers represent the actual data.

The temperature dependent Bézier curves resulted from our algorithm compared with the actual data are introduced in Figure 15. Once again, the results show a very good correlation between the modeled data and the actual data.

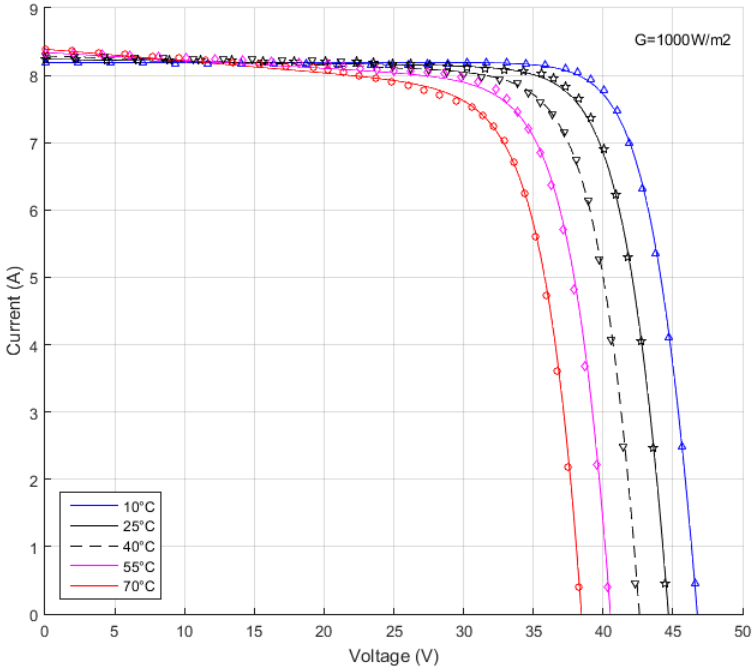

Figure 15. Bézier approximation of the I-V temperature dependent characteristics for the MSMD290AS-36_EU Monocrystalline PV module. The lines represent the computed curves, whereas the markers represent the actual data.

Preprints (www.preprints.org) | NOT PEER-REVIEWED | Posted: 2 February 2018 doi:10.20944/preprints201802.0014.v1

5. Discussion

In all studied cases, the x coordinates can be evenly spaced. Both for the PV cell and for the PV module, the first Bézier cubic curve was very close to a straight line and ended at $x_{03} = 0.5V_{oc}$. The middle curve ended at $x_{13} = 0.75V_{oc}$ for the PV cell and at $0.8V_{oc}$ for the PV module. The relative error is below 1% in the 0 … 0.94 V_{oc} range for the studied PV cell, and the overall absolute error is less than 72mA, for $I_{sc,ref} = 9.207$A.

The differences between the results obtained with the proposed method and the least squares method are negligible (less than 1% for all coordinates). R_s and R_{sh} can be easily derived from the manufacturer's datasheet, using for example the method proposed by Vilallva et al. [4]. In most cases $R_{sh} \approx R_{sho}$; for the PV cell analyzed here, $R_{sh} = 73.19\Omega$, while $R_{sh0} = 73.18\Omega$. Larger differences occur for the series parasitic resistance: for the same PV cell, $R_s = 3.8m\Omega$, while $R_{s0} = 7.2m\Omega$. For different irradiances and temperatures, the section 4.4 provides all the necessary formulae.

6. Conclusions

A novel method for modeling a PV cell or a PV module I-V characteristic has been introduced. To the best of our knowledge, Bézier curves were not used to model the I-V characteristic of PV devices before. The method proved good accuracy and was validated both in the case of a single PV cell and in the case of a whole PV module. The method was also used in the case of varying irradiance and temperature. The proposed method can be used for implementing hardware solar array simulators, for teaching or remote study. It is far more easy to use the proposed method to find the I-V characteristic of a PV cell or module when compared with solving the exponential equations associated with the single or double diode model largely used today.

The advantage of our method relies in the ease of I-V characteristic generation: if we exclude V_{oc} and I_{sc}, only 16 different values (coordinates) have to be stored – SAS manufacturers usually use 1024 double points to accurately define the I-V characteristic. Furthermore, little knowledge of the device itself is required, as only common data from the datasheet is needed.

Acknowledgments: This work was supported by both the Romanian National Authority for Scientific Research and Innovation, CNCS/CCCDI-UEFISCDI within PNCDI III, project number PN-III-P2-2.1-PED-2016-0074 and by Politehnica University Timisoara, according to the Administration Board research policy.

Author Contributions: Both authors have contributed to this research. Aurel Gontean conceived and designed the study and carried out the simulations. Roland Szabo analyzed the data. Aurel Gontean wrote the paper and reviewed the manuscript. Both authors read and approved the manuscript.

Conflicts of Interest: The authors declare no conflict of interest.

Nomenclature

Main Symbols

a	Diode ideality factor
G	Actual irradiance
G_{ref}	Reference irradiance, 1000 W/m²
I	Output current
I_{mp}	Output current at maximum power point
I_{sc}	Short circuit current
$I_{sc,ref}$	Short circuit current 25°C
k	Boltzmann constant
k_I	Current temperature coefficient, A/K
k_V	Voltage temperature coefficient, V/K
$k_{R_{sh}}$	R_{sh} temperature exponent
n_s	Number of series cells
$P_{mp} = V_{mp}I_{mp}$	Maximum output power

 doi:10.20944/preprints201802.0014.v1

q	Electron charge
R_s	Series resistance
$R_{s,ref}$	Series resistance at 25°C
R_{s0}	Series resistance based on I-V characteristic slope close to V_{oc}
R_{sh}	Parallel (shunt) resistance
$R_{sh,ref}$	Parallel (shunt) resistance, at 25°C
R_{sh0}	Parallel (shunt) resistance based on I-V characteristic slope close to I_{sc}
T	Internal temperature, [K]
T_{ref}	Reference temperature 298.15 K
$\Delta T = T - T_{ref}$	Temperature difference
V	Output voltage
V_{oc}	Open circuit voltage
$V_{oc,ref}$	Open circuit reference voltage at 25°C
$V_{oc,cell}$	Solar cell open circuit voltage
$V_{oc,cell,ref}$	Solar cell open circuit reference voltage at 25°C
V_{mp}	Output voltage at maximum power point

Abbreviations

AM	Air Mass
MPP	Maximum power point
PV	Photovoltaic
SAS	Solar Array Simulator
STC	Standard Test Conditions (cell temp. 25°C; irradiance 1000 W/m²; air mass 1.5)

Greek Symbols

α_{Rs}	Series resistance temperature coefficient (linear law)

References

1. 4Q 2017 Frontier Power Market Outlook, https://about.bnef.com/blog/4q-2017-frontier-power-market-outlook/ (accessed on 3 January 2018).
2. Solar PV 2018, https://www.pv-magazine.com/2017/12/01/solar-pv-2018-installs-of-111-gw-a-polysilicon-factory-boom-and-0-30w-for-modules-2/ (accessed on 3 January 2018).
3. Phang, J.C.H.; Chan, D.S.H.; Phillips, J.R. Accurate Analytical Method For The Extraction Of Solar Cell Model Parameters, Electron Lett **1984**, 20(10), pp. 406 – 408, DOI: 10.1049/el:19840281.
4. Villalva, M.G.; Gazoli, J.R.; Filho, E.R. Comprehensive Approach to Modeling and Simulation of Photovoltaic Arrays, *IEEE Trans. Power Electr.* **2009**, 24, pp. 1198–1208.
5. Cubas, J.; Pindado, S.; de Manuel, C. Explicit Expressions for Solar Panel Equivalent Circuit Parameters Based on Analytical Formulation and the Lambert W-Function, *Energies* **2014**, 7, pp. 4098–4115.
6. Chander, S.; Purohit, A.; Sharma, A. Nehra, S.P.; Dhaka, M.S., A study on photovoltaic parameters of mono-crystalline silicon solar cell with cell temperature, *Energy Rep.* **2015**, 1, pp. 104–109.
7. Ishaque, K.; Salam, Z. An improved modeling method to determine the model parameters of photovoltaic (PV) modules using differential evolution (DE), *Sol Energy* **2011**, 85(9), pp. 2349 – 2359, DOI: 10.1016/j.solener.2011.06.025.
8. Gontean, A.; Lica, S.; Bularka, S.; Szabo, R.; Lascu, D. A Novel High Accuracy PV Cell Model Including Self Heating and Parameter Variation, *Energies* **2018**, 11, 36, doi:10.3390/en11010036.
9. Farin, G. A History of Curves and Surfaces in CAGD, in *Handbook of Computer Aided Geometric Design*; Farin, G.E.; Hoschek, J., Kim, M.S. Eds.; Elsevier, Amsterdam, The Netherlands, 2002; pp. 1–22, ISBN 978-0-444-51104-1, https://doi.org/10.1016/B978-0-444-51104-1.50035-6.
10. Farin, G. *Curves and Surfaces for CAGD. A Practical Guide*, 5th Edition, Academic Press, San Francisco, CA, USA, 2002, pp. 81 – 95, ISBN: 1-55860-737-4, https://doi.org/10.1016/B978-1-55860-737-8.50032-6.
11. Mortenson, M.E. *Geometric modeling*, 3rd Edition, Industrial Press, South Norwalk CT, USA 2006, ISBN 978-0-831-13298-9.

12. Farin, G. Shape Representation, in *Wiley Encyclopedia of Electrical and Electronics Engineering*, Published Online: 13 Jul 2007, http://onlinelibrary.wiley.com/doi/10.1002/047134608X.W7525.pub2/full, ISBN: 978-0-471-34608-1, DOI: 10.1002/047134608X.
13. Tromba, D.; Munteanu, L.; Schneider, V.; Holzapfel, F. Approach trajectory generation using Bézier curves, 2015 IEEE International Conference on Aerospace Electronics and Remote Sensing Technology (ICARES), 3-5 Dec. 2015, DOI: 10.1109/ICARES.2015.7429835
14. Jalba, A.C.; Wilkinson, M.; Roerdink J. Shape representation and recognition through morphological curvature scale spaces, *IEEE Trans Image Process*, 2006 15 (2), pp. 331 - 341, DOI: 10.1109/TIP.2005.860606.
15. Prautzsch, H.; Boehm, W.; Paluszny M. *Bézier and B-Spline Techniques*, Spinger, Berlin, Germany, 2002, pp. 9 – 57, ISBN 3-540-43761-4.
16. 156 mm Monocrystalline Mono Solar Cell 6 x 6. Available online: https://www.aliexpress.com/item/50pcs-lot-4-6W-156mm-mono-solar-cells-6x6-150feet-Tabbing-Wire-15feet-Busbar-Wire-1pc/1932804007.html (accessed on 21 Sep 2017).
17. MünchenSolar M Series Monocrystalline MSMDxxxAS-36.EU Datasheet, https://cdn.enf.com.cn/Product/pdf/Crystalline/559cd7e85436f.pdf (accessed on 31 Jan 2018)
18. Mugnaini, D. Bézier Curve with draggable control points. Draw, manipulate and reconstruct Bézier Curves, version 1.11, Available online: https://www.mathworks.com/matlabcentral/fileexchange/51046-bézier-curve-with-draggable-control-points (accessed on 30 Dec 2017)
19. Garrity, M. Bézier Curves and Kronecker's Tensor Product, posted 13 October 2014, Available online: https://blogs.mathworks.com/graphics/2014/10/13/bézier-curves/, (accessed on 31 Dec 2017)
20. Khan, M. Cubic Bézier Least Square Fitting, version 1.4, https://www.mathworks.com/matlabcentral/fileexchange/15542-cubic-bézier-least-square-fitting, (accessed on 30 December 2017).
21. Wolberg, J. *Data Analysis Using the Method of Least Squares. Extracting the Most Information from Experiments*, 2006 Springer-Verlag Berlin Heidelberg, ISBN 978-3-540-25674-8, DOI 10.1007/3-540-31720-1
22. Hansen pC.; Pereyra V.; Scherer G. *Least Squares Data Fitting with Applications*, JHU Press, Baltimore, USA, 2013, ISBN 978-1-421-40786-9.
23. Shao, L.; Zhou, H. Curve Fitting with Bézier Cubics, in *Graphical Models and Image Processing*, Volume 58, Issue 3, May 1996, Pages 223-232, https://doi.org/10.1006/gmip.1996.0019.
24. Zhao, L.; Jiang, J.; Song, C.; Bao, L.; Gao, J., Parameter Optimization for Bézier Curve Fitting Based on Genetic Algorithm, in: Tan Y., Shi Y., Mo H. (eds) *Advances in Swarm Intelligence*, ICSI 2013, Lecture Notes in Computer Science, vol 7928. Springer, Berlin, DOI: https://doi.org/10.1007/978-3-642-38703-6_53.